Scaling Behavior of Dilute Polymer Solutions Confined between Parallel Plates

J. H. van Vliet, M. C. Luyten, and G. ten Brinke*

Department of Polymer Chemistry, University of Groningen, Nijenborgh 16, 9747 AG Groningen, The Netherlands

Received December 26, 1991; Revised Manuscript Received April 2, 1992

ABSTRACT: The average size and shape of a polymer coil confined in a slit between two parallel plates depends on the distance L between the plates. On the basis of numerical results, four different regimes can be distinguished. For large values of L the coil is essentially unconfined. For intermediate values the coil orientates without being squeezed considerably. For still smaller values the coil is squeezed with a corresponding decrease in the value of the radius of gyration. A further reduction in slit width is accompanied by a sharp increase in the value of the radius of gyration, signaling the onset of the transition from three- to two-dimensional behavior. L-Dependent scaling relations are supposed to be valid in the latter regime. Using Monte Carlo results for self-avoiding walks on a cubic lattice, scaling predictions for the parallel component of the radius of gyration and the end-to-end point distance as well as for the osmotic pressure and the number of segments at the wall are presented and verified.

Introduction

The static and dynamic properties of polymer solutions are considerably influenced by confinement of the polymer chains, e.g., between two parallel walls in a slit or in a cylindrical pore. The effects of confinement are of relevance in several applications as in size-exclusion and hydrodynamic chromatography,[1,2] drag reduction,[3,4] enhanced oil recovery,[5] and stabilization of colloidal dispersions.[6-8] The interference between polymer coil and confinement is complicated by the fact that the average shape of a polymer coil is distinctly asymmetric, an asymmetry that arises from the infinite variety of irregular conformations the chain can assume compared to the number of conformations possessing any element of symmetry.[9] A three-dimensional coil can best be visualized as a "cake of soap", the average shape being characterized by the conformational average of the eigenvalues of the radius of gyration matrix called principal components. They are in descending order denoted as $\langle\lambda_1\rangle$, $\langle\lambda_2\rangle$, and $\langle\lambda_3\rangle$ and are related to the mean-square radius of gyration $\langle R_g^2\rangle$ by

$$\langle R_g^2\rangle = \langle\lambda_1\rangle + \langle\lambda_2\rangle + \langle\lambda_3\rangle \tag{1}$$

For three-dimensional self-avoiding walks (SAW) they satisfy[10]

$$\langle\lambda_1\rangle:\langle\lambda_2\rangle:\langle\lambda_3\rangle = 14.8:3.06:1 \tag{2}$$

Several consequences of the interference between the anisotropic shape of the polymer coil and the spatial confinement have been discussed in previous publications.[11-13] Monte Carlo simulations of dilute polymer solutions in a good solvent confined between two parallel plates show that as a function of plate distance L the coil starts to orientate long before any noticeable change in size is observed.[11] Actually four different regimes can be distinguished. In regime IV the plate distance is large and the system behaves essentially unconfined. A sufficient reduction in plate distance brings the system in regime III, where the coil orientates with the longest and later also the middle principal axis parallel to the plates. The crossover between regimes III and II occurs when the coil really becomes squeezed, the onset of which is signaled by a decrease in the value of all three principal components and therefore of the radius of gyration itself. This, of course, cannot go on indefinitely due to the increasing excluded-volume effect, and, finally, regime I is entered, where the value of the radius of gyration as well as of the largest and the middle principal components start to increase abruptly toward their two-dimensional value. At the same time, the value of the smallest principal component decreases sharply toward zero. It is in this last regime (I), where an interesting scaling behavior for various physical quantities might be expected and in fact has been proposed.[14,15]

The discussion here is limited to the static properties of dilute solutions of polymer chains confined in a slit in the absence of interactions with the wall. The dynamical properties, notably the intrinsic viscosity, have been investigated as well. Interesting differences between the influences of the confinement on the intrinsic viscosity of Couette and Poiseuille flow were found.[12,13] In a Couette flow the intrinsic viscosity drops sharply from its unconfined value at distances between the plates for which the coils are deformed, i.e., regimes II and I. For a Poiseuille flow, on the other hand, it starts to decrease gradually already at much larger plate distances, far into regime IV. This is explained by the fact that the polymers have a tendency to concentrate near the center of the slit where, different from Couette flow, in Poiseuille flow the shear rate vanishes. However, these dynamic properties do not seem to show an interesting scaling behavior, and for this reason are not considered here.

This paper is devoted to polymer chains in an athermal solvent confined to a slit. The boundaries are two parallel plates a distance L apart. Values of L considered will be less than the characteristic length of the polymer coil, ξ. A customary identification of ξ is with the root-mean-square end-to-end distance, $\langle R^2\rangle^{1/2}$, or root-mean-square radius of gyration, $\langle R_g^2\rangle^{1/2}$, of the coil. Daoud and de Gennes[14,15] predicted the following scaling behavior for the component of ξ parallel to the walls, $\xi_\parallel$, in the regime $\xi > L$

$$\xi_\parallel \sim N^{\nu(2)}L^{-[\nu(2)/\nu(3)-1]} \tag{3}$$

where $\nu(3)$ and $\nu(2)$ are the well-known excluded-volume exponents of any quantity that characterizes the size of the polymer coil in three- and two-dimensional space, respectively, and N is the number of chain segments. A similar relation is found for a tube geometry except that $\nu(2)$ has to be replaced by the one-dimensional value $\nu(1)$

0024-9297/92/2225-3802$03.00/0

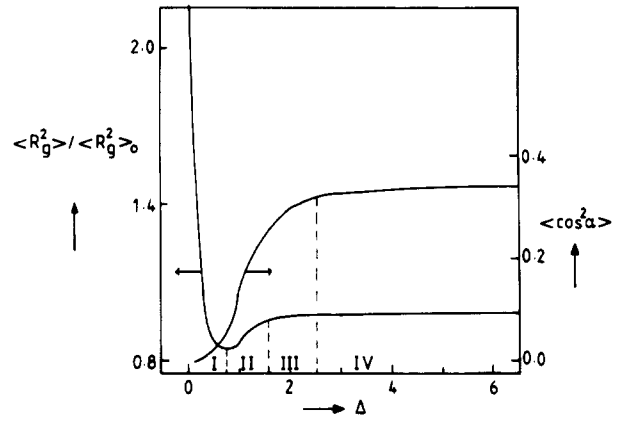

Figure 1. Illustration of the definition of the various regimes based on the schematic behavior of $\langle R_g^2\rangle/\langle R_g^2\rangle_0$, the ratio between the value of the mean-square radius of gyration in the confined and the unconfined situation, and $\langle\cos^2\alpha\rangle$, the orientation function of the longest principal component, as a function of $\Delta = L/N^{0.6}$.

= 1. As is well-known, the general expression for the Flory exponent is given by $\nu(d) = 3/(d+2)$. In several publications the agreement between eq 3, exact enumeration, and Monte Carlo simulation results is found to be satisfactory.[16-19] Monte Carlo results for self-avoiding walks in tubes are also found to satisfy the corresponding scaling.[20]

A basic problem is the definition of the exact regime where the transition between three-dimensional and two-dimensional behavior occurs and where the scaling relations are supposed to hold. The problem is analyzed here in terms of a scaled distance Δ between the walls, where Δ is defined as

$$\Delta \equiv L/N^{\nu(3)} \tag{4}$$

In a previous publication[11] we showed that the polymer coil, being an ellipsoidal shaped object, orientates for $\Delta \leq 2.5$. It is squeezed for $\Delta \leq 1.5$. The squeezing starts with a decrease of the mean-square radius of gyration $\langle R_g^2\rangle$ and its principal components. Eventually, when $\Delta \leq 1$, the values for the square radius of gyration and the two largest principal components increase until the limiting two-dimensional values for these quantities are reached for $\Delta \to 0$. In the limit $\Delta \to 0$ the smallest principal component disappears. A minimum of $\langle R_g^2\rangle$ and its principal components as a function of Δ is found at $\Delta_{min} \approx 1$. A smaller minimum is also found for the end-to-end distance as a function of L by Monte Carlo studies[21] and exact enumeration methods.[16]

From this discussion it is clear that the four regimes mentioned before can in terms of Δ be defined as follows:

Regime IV ($\Delta \geq 2.5$): The conformations of the polymer coil are on the average not influenced by the presence of the walls.

Regime III ($1.5 \leq \Delta \leq 2.5$): The coil starts to orientate, but the average shape is still close to the unconfined situation.

Regime II ($1 \leq \Delta \leq 1.5$): The values of all three principal components are reduced; the coil is squeezed.

Regime I ($\Delta \leq 1$): The coil is deformed even more, and the characteristic lengths of the chain, e.g., the radius of gyration, its principal components, and the end-to-end distance, monotonously go to their two-dimensional values.

Figure 1 gives an illustration of the various regimes. In this paper regimes I and II are considered in some detail. A priori it is clear that eq 3 is unambiguously applicable only to regime I. Scaling equations for the osmotic pressure and the monomer density at the wall for the same regime I will be introduced in the next section.

Scaling Relations

The border between regimes I and II is defined by the minimum in the characteristic size of the polymer coil. As shown before, this minimum occurs at $\Delta_{min} \approx 1$ and hence

$$L_{min} \simeq N^{\nu(3)} \tag{5}$$

This scaling behavior of L_{min} is found from the Monte Carlo data of $\langle R_g^2\rangle$ and $\langle R^2\rangle$ for SAW's on a cubic lattice for a wide range of chain lengths, the number of steps, N, of the SAW's varying from $N = 19$ to $N = 639$.[11] For a Monte Carlo simulation study of SAW's confined in a slit on a tetrahedral lattice Ishinabe[18] found that the value of L for which $\langle R^2\rangle$ reaches its minimum is a linear function of N for values of N ranging from 10 to 100. This difference is probably due to the limited range of chain lengths considered.

The scaling of the reduced osmotic pressure $\Pi^* = \Pi/k_BT$ of a single coil in a slit can be derived from the equation for the reduced free energy $f^* = f/k_BT$ of a single coil, which, according to Daoud and de Gennes,[14,15] is given by

$$f^* \sim NL^{-1/\nu(3)} \tag{6}$$

and hence

$$\Pi^* = -\frac{\partial f^*}{A\,\partial L} \sim NL^{-[1/\nu(3)+1]} \tag{7}$$

where A is the surface area of the boundary walls. For the case of a confined random walk, the osmotic pressure is known exactly[22] and is given by

$$\Pi^* = \frac{\pi^2 Nb^2}{3AL^3} \tag{8}$$

where b is the step length of the random walk and A is the surface of the two confining parallel plates situated at a distance L from each other. Comparison of eq 7 and 8 shows that they agree for $\nu(3) = 0.5$, the random walk value.

Closely related to the osmotic pressure is the density of monomers at the plate. In a continuous system, as opposed to the lattice model employed here, the osmotic pressure in a confined system is related to the monomer density at the walls by the so-called *wall theorem*,[23,24] which asserts that the density of monomers at contact with the wall, $\rho(0)$, is related to the osmotic pressure Π and temperature T by the ideal gas equation; i.e.

$$\Pi = k_BT\rho(0) \tag{9}$$

The validity of this equation automatically implies that Π and $\rho(0)$ satisfy the same scaling relations. For a lattice model eq 8 is no longer valid and has to be replaced by an expression first derived by Dickman[25] and which will be discussed in some detail in the next section. Here we only notice that as long as the system is sufficiently dilute, as is obviously the case for a single chain in a good solvent, the fact that a lattice is used to simulate the system seems not a real restriction. Consequently, for this case we expect the same scaling behavior for $\langle\rho(1)\rangle$ and Π, i.e.

$$\langle\rho(1)\rangle \sim NL^{-[1/\nu(3)+1]} \tag{10}$$

where the argument 1 indicates the lattice layer adjacent to the plate and $\langle\ \rangle$ denotes the average over all possible conformations.

Model and Simulation Method

Monte Carlo simulations of a SAW on a simple cubic lattice with periodic boundary conditions in the x- and y-direction were performed. The two parallel walls were perpendicular to the z-axis. The length of the lattice in the directions with periodic boundary conditions varied with the chain length considered. In all cases, this length exceeded the root-mean-square end-to-end distance of the SAW. In the case of the longest chain length, $N = 320$, the length of the lattice in the x- and y-direction was, for instance, 66. The data on osmotic pressures and the number of segments in the lattice layers adjacent to the walls, were obtained for two chain lengths. The number of steps of the SAW's considered were $N = 150$ and $N = 320$. For the shortest distance between the walls the densities, expressed as the fraction of lattice sites occupied, varied between 0.4% for $N = 150$ and 0.9% for $N = 320$. With larger distances between the walls the densities were correspondingly lower. For each chain length considered, the lattice length in the x- and y-direction was fixed. The largest distance between walls for which data were computed was $L = 33$ for $N = 150$ and $L = 41$ for N = 320. For each chain length and distance between the walls, a representative sample was obtained by the reptation algorithm. To speed up equilibration, chain growth and reptation took place simultaneously.

The first 200 000 attempted moves after completion of chain growth were ignored. From the subsequent interval of 80 000 attempted moves 51, at equally spaced intervals, quantities of interest were calculated and averaged afterward. This procedure was repeated for 10–30 independent runs. After averaging again the statistical errors were calculated as usual from the averages per run.

The component of the mean-square radius of gyration, $\langle R_{g\parallel}^2 \rangle$, and the mean-square end-to-end distance, $\langle R_\parallel^2 \rangle$, parallel to the walls were calculated for $\Delta < 1$ (regime I) for eight chain lengths with $N = 19$–639.

The calculation of the reduced osmotic pressure, Π^*, for the lattice chains was performed by a slightly adapted version of Dickman's algorithm.[25,26] In a continuous space model Π^* is given by

$$\Pi^* = K^{-(d-1)} \frac{\partial \ln Q(L)}{\partial L} \tag{11}$$

where $Q(L)$ is the canonical partition function for a slit with diameter L, K is the length of the lattice in the periodic directions, and d is the spatial dimension. For a lattice Dickman replaced eq 8 by its discrete analog

$$\Pi^* = K^{-(d-1)}[\ln Q(L) - \ln Q(L-1)] \tag{12}$$

Equation 12 can be transformed into[25]

$$\Pi^* = K^{-(d-1)} \int_0^1 \frac{\langle m(1,\lambda) \rangle}{\lambda} \, d\lambda \tag{13}$$

Here $m(1,\lambda)$ is the number of monomers in layer 1 adjacent to one of the parallel plates if an additional repulsive potential is present in this layer, giving rise to a factor $\lambda \leq 1$ in the partition function for each monomer in this layer. Expression 13 for the osmotic pressure clearly shows that, at least at high densities, Π^* and $\langle \rho(1) \rangle$ cannot scale in the same way. As pointed out by Dickman,[25] Π^* diverges in the limit of a fully occupied lattice, for which $\rho(1,\lambda) = K^{-(d-1)} m(1,\lambda) = 1$ irrespective of the value of λ. Application of the Metropolis sampling scheme with the aforementioned reptation algorithm to generate configurations of the system can now be used to calculate $\langle m(1,\lambda) \rangle$ for various values of λ and L. Π^* is calculated via numerical integration of eq 13. In the Metropolis procedure each configuration is accepted with probability $p = \min(1, \lambda^{[\Delta m(1)]})$, where $\Delta m(1)$ is the change in the number of segments at $z = 1$ due to this reptation move. Details of the method can be found in Dickman's article[25] and in a review on Monte Carlo simulations of lattice chains and references therein.[26]

Here we will use an adaptation of eqs 12 and 13 because of the very low segment densities considered: at the highest 0.9%, in contrast with Dickman's work where a segment density of at least 23% was used.[25] Equation 12 is replaced by

$$\Pi^* = K^{-(d-1)} \frac{1}{2} [\ln Q(L) - \ln Q(L-2)] \tag{14}$$

and eq 13 by

$$\Pi^* = K^{-(d-1)} \frac{1}{2} \int_0^1 \frac{M(\lambda)}{\lambda} \, d\lambda \tag{15}$$

with $M(\lambda) = \langle m(1,\lambda) \rangle + \langle m(L-1,\lambda) \rangle$, and $m(L-1,\lambda)$ is the number of segments in the lattice layer at $z = L - 1$, near the wall at $z = L$, for a given conformation and a given value of λ. Of course, the repulsive potential is now applied to both boundary layers. It is clear that the numerical accuracy of eq 14 is less than that of eq 12, since the differentiation step is twice as large as that in eq 12. The number of segments used in eq 15 is on average twice as large as that in eq 13. Therefore, with eq 15 statistical errors in Π^* are less than with eq 13. For the very low segment densities dealt with here, the use of eq 15 is preferred. Then the acceptance probability of a configuration in the Metropolis procedure should be modified to $p = \min(1, \lambda^{\Delta M})$, where ΔM is the change in the number of segments at $z = 1$ and $z = L - 1$ accompanying the attempted reptation move.

The values of $M(\lambda)/\lambda$ were obtained for 10 values of λ, $\lambda = 0.1, 0.2, 0.3, \ldots, 1$. The number of independent runs was varied from 10 to 30, in descending order for λ and in ascending order for L. In this order the segment density at the walls decreases. Hence, an increasing number of runs is needed to get reliable results for $M(\lambda)/\lambda$.

The results of the Monte Carlo simulations are used to obtain scaling relations as a function of the chain length N and the slit width L. The scaling exponents were obtained by linear regression according to

$$\langle \ln (J) \rangle = \ln (A) + B \ln (I) \tag{16}$$

where J is the measured quantity, I is the independent variable (here L or N), A is the intercept of the line, and B is the scaling exponent for J as a function of I. The values of I are exactly known; the values of $\langle J \rangle$ have a statistical error (standard derivation) σ_J. From elementary statistics it follows that $\langle \ln (J) \rangle$ and its statistical error, $\sigma_{\ln (J)}$ ($\sigma_J / \langle J \rangle \ll 1$), are

$$\langle \ln (J) \rangle \approx \ln (J) - \frac{1}{2}\sigma_{\ln (J)}^2 \qquad \sigma_{\ln (J)}^2 \approx \frac{\sigma_J^2}{\langle J \rangle^2} \tag{17}$$

The values of $\langle \ln (J) \rangle$ and $\sigma_{\ln (J)}$ obtained by eq 17 were used in the linear regression procedure. The numerical procedure to perform the linear regression as well as the ways to judge the goodness of the fit is described in *Numerical Recipes* and references therein.[27]

Simulation Results and Discussion

The scaling exponents obtained are presented in Table I. The values of $\langle R_{g\parallel}^2 \rangle$ and $\langle R_\parallel^2 \rangle$ were obtained for $\Delta < 1$. The results are presented in Table II. The scaling exponent with respect to N for $\xi_\parallel^2$ is expected to be $\omega =$

Table I
Scaling Exponents[a]

	scaling equations			data	
	L	N		L	N
$\langle R_\parallel^2 \rangle$	$-2[\nu(2)/\nu(3) - 1]$	$2\nu(2)$	MC	-0.55 ± 0.04	1.47 ± 0.03
			FL	-0.5	1.5
$\langle R_{g\parallel}^2 \rangle$	$-2[\nu(2)/\nu(3) - 1]$	$2\nu(2)$	MC	-0.54 ± 0.02	1.45 ± 0.02
			FL	-0.5	1.5
$\langle \rho(1) \rangle/N$	$-\frac{[\nu(3)+1]}{\nu(3)}$	0	MC	-2.51 ± 0.07	
			FL	-2.67	0
Π^*/N	$-\frac{[\nu(3)+1]}{\nu(3)}$	0	MC	-2.76 ± 0.04	
			FL	-2.67	0

[a] MC indicates the Monte Carlo results; FL indicates the results with $\nu(2) = {}^3/_4$ and $\nu(3) = {}^3/_5$ substituted in the scaling equations.

Table II
Parallel Components of S^2 and R^2

N	L	$\langle R_\parallel^2 \rangle$	$\langle S_\parallel^2 \rangle$
19	3	20 ± 2	3.1 ± 0.2
19	5	14 ± 2	2.3 ± 0.1
39	3	54 ± 5	8.4 ± 0.3
39	5	42 ± 4	6.2 ± 0.4
59	5	71 ± 7	10.9 ± 0.8
59	9	58 ± 6	8.99 ± 0.6
79	3	158 ± 23	22.7 ± 1.6
79	5	123 ± 11	17.6 ± 1.0
79	9	81 ± 7	12.7 ± 0.6
150	5	317 ± 32	43.4 ± 2.1
150	9	203 ± 27	31.5 ± 2.2
150	17	184 ± 22	27.4 ± 2.0
159	3	445 ± 27	66.2 ± 1.4
159	5	312 ± 58	48.1 ± 6.1
159	9	232 ± 25	33.7 ± 1.4
159	17	181 ± 16	29.2 ± 2.4
319	5	913 ± 83	128.5 ± 11.8
319	9	649 ± 78	91.8 ± 10.1
319	17	428 ± 34	65.2 ± 4.6
639	5	2592 ± 355	387.2 ± 37.0
639	9	1833 ± 376	269.0 ± 42.0
639	17	1372 ± 302	197.7 ± 35.5
639	33	963 ± 179	143.0 ± 19.1

$2\nu(2)$. With respect to L the scaling exponent for $\xi_\parallel^2$ is expected to be $\theta = -2[\nu(2)/\nu(3) - 1]$ (eq 1). The Flory exponents were substituted in the equations for ω and θ. These values of ω and θ were used as starting values in an iterative procedure to obtain precise values of ω and θ. First, $\langle \ln (R_{g\parallel}^2/N^\omega) \rangle$ and $\langle \ln (R_\parallel^2/N^\omega) \rangle$ are fitted against $\ln (L)$, obtaining an estimated value for the scaling exponent, θ, of L. Then, θ is used to get an improved value of ω in a fit of $\langle \ln (R_{g\parallel}^2 L^{-\theta}) \rangle$ and $\langle \ln (R_\parallel^2 L^{-\theta}) \rangle$ against $\ln (N)$. The next iteration step starts with a fit of $\langle \ln (R_{g\parallel}^2/N^\omega) \rangle$ and $\langle \ln (R_\parallel^2/N^\omega) \rangle$ against $\ln (L)$, with the use of the improved scaling exponent ω. The criterion to stop the iteration is that the change in the value of both ω and θ from one fit to the comparable fit in the next iteration is smaller than the smallest statistical significant digit. This point is reached here after two iteration steps. The procedure of course can also be started the other way around: initializing the iteration with a fit of $\langle \ln (R_{g\parallel}^2 L^{-\theta}) \rangle$ and $\langle \ln (R_\parallel^2 L^{-\theta}) \rangle$ against $\ln (N)$. The same final results for θ and ω were obtained then, within the same number of iteration steps.

From Table I it is clear that values for both ω and θ are close to the values which are obtained by substitution of the Flory exponents in eq 1. This was already observed before for both lattice[16-18] and off-lattice chains.[19] The data presented here are, however, more conclusive. First, the regime for which eq 1 is valid is explicitly recognized to be regime I with $\Delta < 1$. Second, the range of chain lengths and slit widths is much larger than has been studied so far. Third, we present values for both ω and θ for $\langle R_{g\parallel}^2 \rangle$ as well as $\langle R_\parallel^2 \rangle$. So far θ only has been given for $\langle R^2 \rangle$ and not for $\langle R_\parallel^2 \rangle$, but $\langle R_{g\parallel}^2 \rangle$ and $\langle R_\parallel^2 \rangle$ are the relevant quantities and not $\langle R_g^2 \rangle$ and $\langle R^2 \rangle$ (eq 1).[13,14] Nevertheless, for very long chains and very small slit widths one would expect the same results for the scaling exponents θ and ω, irrespective of whether $\langle R_{g\parallel}^2 \rangle$ and $\langle R_\parallel^2 \rangle$ or $\langle R_g^2 \rangle$ and $\langle R^2 \rangle$ are used. Convergence to the correct scaling exponents, however, might occur for shorter chains and larger slit widths with the proper quantities.

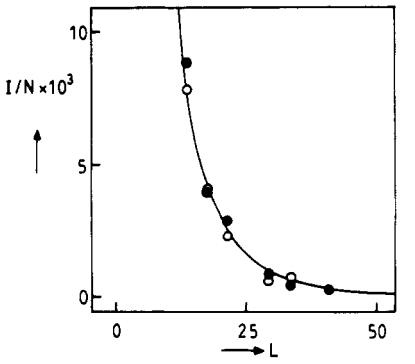

Figure 2. I/N as a function of L: (○) $N = 150$; (●) $N = 320$. For $L = 9$ data points not shown are $N = 150$, $I/N = 2.42 \times 10^{-2}$ and $N = 320$, $I/N = 2.34 \times 10^{-2}$.

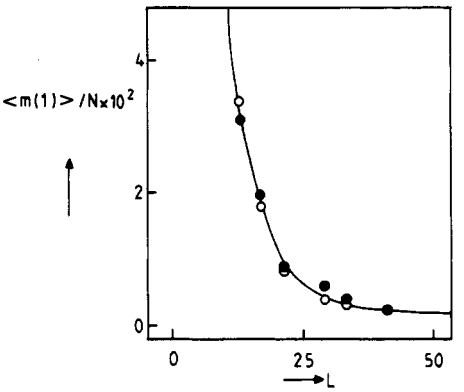

Figure 3. $\langle m(1) \rangle/N$ as a function of L: (○) $N = 150$; (●) = 320. For $L = 9$ data points not shown are $N = 150$, $\langle m(1) \rangle/N = 7.4 \times 10^{-2}$, and $N = 320$, $\langle m(1) \rangle/N = 7.9 \times 10^{-2}$.

In Figure 2 I/N is plotted against L, with $\Pi^* \sim I$ and I equal to the integral over $M(\lambda)/\lambda$ in eq 15. From Figure 2 it is clear that data for $N = 150$ and for $N = 320$ neatly collapse on a single universal curve as expected from eq 7. The values of Π^*/N for $N = 150$, and N = 320 available for a single slit width, were averaged and used in the calculation of the statistical error in the average value. The so averaged values of Π^*/N were used to obtain the scaling exponent with respect to L (eqs 16 and 17). The fit is performed for seven averaged data points (see also Figure 2). The scaling exponent is slightly higher than the exponent calculated with the Flory exponents (Table I). It should be noted that Π^* increases with decreasing L, in both regimes II and I.

Recent lattice Monte Carlo simulations on polymer systems corroborated scaling predictions of osmotic pressure related quantities,[28-30] which gives confidence in Dickman's[25] procedure for the calculation of Π^*. Qualitatively, our Monte Carlo data on the osmotic pressure are in agreement with data on the free energy obtained by an exact enumeration method.[31]

In Figure 3, the normalized average number of monomers in the lattice plane adjacent to the wall $\langle m(1) \rangle/N$ is plotted against L. Also here data for $N = 150$ and $N = 320$ nicely collapse on a single universal curve as expected from eq

9. The fit is performed with eight data points with statistical errors from Monte Carlo simulations: three data points for $N = 150$ and five data points for $N = 320$. The Monte Carlo result for the scaling exponent of $\langle\rho(1)\rangle/N$ is close to the theoretical predicted value (Table I). Hence, it seems that at least at sufficient low concentration the osmotic pressure Π and the monomer density at the wall scale in the same manner. This is not unreasonable since the lattice character of the system is most likely to manifest itself at higher concentrations only. As long as the average distance between the monomers in the layers adjacent to the walls is much larger than the lattice distance, a lattice model is probably not too bad an approximation for the continuous system. However, even at these low densities we observe, as in ref 28, a decrease in the value of $\langle\rho(1)\rangle/\Pi^*$ as a function of Π^*, which is reflected in the small difference in the exponent of the L-dependence of $\langle\rho(1)\rangle/N$ and Π^*/N (Table I).

Concluding Remarks

Since in our simulations the subspace of the slit perpendicular to the constraint is supposed to be infinite, one should be careful not to introduce finite size effects due to the periodic boundary conditions of the lattice.[32] There is excellent agreement between scaling predictions on $\langle R_{g\parallel}^2\rangle$ and $\langle R_\parallel^2\rangle$ and the Monte Carlo results for a rather extensive batch of data. Therefore, the requirement that the length of the lattice in the periodic directions is larger than the root-mean-square end-to-end distance of the SAW seems a sufficient condition to assure virtual infiniteness of the periodic subspace of the lattice.

The scaling exponents for the osmotic pressure and the number of segments at the wall obtained by Monte Carlo simulations are in good agreement with scaling predictions using the Flory exponent $\nu(d) = 3/(d+2)$. For the osmotic pressure and the number of segments at the walls, scaling exponents for N were not obtained explicitly, since only two chain lengths were studied. Nevertheless, from Figures 2 and 3 it is clear that the osmotic pressure and the number of segments divided by N collapse neatly on a single curve for the two different chain lengths. This indicates that the scaling exponent with respect to N equals 1, as expected from eqs 7 and 10.

References and Notes

(1) Small, H. *J. Colloid Interface Sci.* **1974**, *48*, 147.
(2) Di Marzio, E. A.; Guttman, C. M. *Macromolecules* **1970**, *3*, 131.
(3) Zakin, J. L.; Hunston, D. L. *J. Macromol. Sci., Phys.* **1980**, *B18*, 795.
(4) Block, H. *Molecular Behavior and the Development of Polymeric Materials*; Ledwith, A., North, A. M., Eds.; Chapman & Hall: London, 1975.
(5) Chauveteau, G., Tirrell, M.; Omari, A. *J. Colloid Interface Sci.* **1984**, *100*, 41.
(6) Vrij, A. *Pure Appl. Chem.* **1976**, *48*, 471.
(7) Naper, D. H. *Polymeric Stabilization of Colloidal Dispersions*; Academic: London, 1983.
(8) Lal, M.; Watson, G. M. *ACS Symp. Ser.* **1984**, *240*, 205.
(9) Solc, K. *Polym. News* **1977**, *4*, 67.
(10) Mazur, J.; Gutman, C. M.; McCrackin, F. L. *Macromolecules* **1973**, *6*, 872.
(11) van Vliet, J. H.; ten Brinke, G. *J. Chem. Phys.* **1990**, *93*, 1436.
(12) van Vliet, J. H.; ten Brinke, G. *Macromolecules* **1991**, *24*, 5351.
(13) van Vliet, J. H.; ten Brinke, G. *Macromolecules*, in press.
(14) Daoud, M.; de Gennes, P.-G. *J. Phys. (Les Ulis, Fr.)* **1977**, *38*, 85.
(15) de Gennes, P.-G. *Scaling Concepts in Polymer Physics*; Cornell University Press: Ithaca, NY, 1979.
(16) Barr, R.; Brender, C.; Lax, M. *J. Chem. Phys.* **1980**, *72*, 2702.
(17) Barr, R.; Brender, C.; Lax, M. *J. Chem. Phys.* **1981**, *75*, 460.
(18) Ishinabe, T. *J. Chem. Phys.* **1985**, *83*, 423.
(19) Webman, I.; Lebowitz, J. L.; Kalos, M. H. *J. Phys. (Les Ulis, Fr.)* **1980**, *41*, 579.
(20) Wall, F. T.; Seitz, W. A.; Chin, J. C.; de Gennes, P.-G. *Proc. Natl. Acad. Sci. U.S.A.* **1978**, *75*, 2069.
(21) Wall, F. T.; Mandel, F.; Chin, J. C. *J. Chem. Phys.* **1976**, *65*, 2231.
(22) Edwards, S. F.; Fried, K. F. *J. Phys.* **1969**, *A2*, 145.
(23) Lovet, R.; Baus, M. *J. Chem. Phys.* **1991**, *95*, 1991.
(24) Dickman, R.; Hall, C. K. *J. Chem. Phys.* **1988**, *89*, 3168.
(25) Dickman, R. *J. Chem. Phys.* **1987**, *87*, 2246.
(26) Kremer, K.; Binder, K. *Comput. Phys. Rep.* **1988**, *7*, 260.
(27) Press, H.; Flannery, B. P.; Teukolsky, S. A.; Vetterling, W. T. *Numerical Recipes*; Cambridge University Press: Cambridge, U.K., 1986.
(28) Hertanto, A.; Dickman, R. *J. Chem. Phys.* **1988**, *89*, 7577.
(29) Dickman, R. *J. Chem. Phys.* **1989**, *91*, 454.
(30) Deutsch, H. P.; Dickman, R. *J. Chem. Phys.* **1990**, *93*, 8983.
(31) Midlerniss, K. M.; Torrie, G. M.; Whittington, S. G. *J. Chem. Phys.* **1977**, *66*, 3227.
(32) Halley, J. W. *J. Chem. Phys.* **1988**, *88*, 5181.